FT-IR, FT-Raman, NBO, HOMO-LUMO analysis and molecular docking study of 5-chloro-N-(2-fluorophenyl)pyrazine-2-carboxamide

FT-IR, FT-Raman, NBO, HOMO-LUMO analysis and molecular docking study of 5-chloro-*N*-(2-fluorophenyl)pyrazine-2-carboxamide

K. S. Resmi[a], C. Yohannan Panicker[a,*], Jan Zitko[b], Martin Dolezal[b], Javeed Ahmad War[c], S. K. Srivastava[c], C. Van Alsenoy[d]

[a] *Department of Physics, TKM College of Arts and Science, Kollam, Kerala, India*
[b] *Faculty of Pharmacy in Hradec Kralove, Charles University in Prague, Heyrovskeho 1203, Hradec Kralove, 500 05, Czech Republic*
[c] *Department of Chemistry, Dr.H.S.Gour Central University, Sagar, M. P. India*
[d] *Structural Chemistry Group, Department of Chemistry, University of Antwerp, Groenenborgerlaan 171, B-2020 Antwerp, Belgium*

[*] *Author for correspondence: C. Yohannan Panicker, email: cyphyp@rediffmail.com*
Received 29 Apr 2015; Accepted 23 Jun 2015; Available Online 23 Jun 2015

Abstract

In this work, the vibrational spectral analysis was carried out by using FT-Raman and FT-IR spectroscopy of 5-chloro-*N*-(2-fluorophenyl)pyrazine-2-carboxamide. Theoretical calculations were performed by using Density Functional Theory (DFT). The complete vibrational assignments of wavenumbers were made on the basis of potential energy distribution. The calculated wavenumbers were applied to simulate spectra of the title compound, which show excellent agreement with observed spectra. The frontier orbital energy gap and related properties of the molecule illustrate the reactivity of the title compound. The hyperpolarizability of the title compound was calculated and was in good agreement with similar derivatives. Stability of the molecule arising from hyper-conjugative interactions and charge delocalization was analysed using natural bond orbital analysis. From MEP plot, it is evident that the negative charge covers the C=O group and the positive region is over the NH group. Molecular docking studies suggest that the compound might exhibit inhibitory activity against ACP reductase.

Keywords: DFT; FT-IR; FT-Raman; Pyrazine; Molecular docking

1. Introduction

The pyrazine ring is a part of many polycyclic compounds of biological and industrial significance. Some of its derivatives are used as anti-glaucomatic [1], anti-convulsant [2], antiviral [3], anti-mycobacterial [4-6], and antifungal [7] agents, antagonist in pain treatment [8], inhibitors in type 2 diabetes mellitus [9], spleen tyrosine kinase (is a cytosolic non-receptor protein) inhibitors [10], as potent inhibitors of apoptosis proteins antagonists [11], fluorescents [12] and are available as building blocks for pharmaceuticals [13]. A series of Schiff base derivatives containing pyrazine exerted antibacterial activity against *E-scherichia coli, Pseudomonas-aeruginosa, Staphylococcus-aureus, Bacillus-subtilis and B.-amyloliquefaciens* [14]. Novel pyrido[2,3-*b*]pyrazines substituted in position 7 with nitrogen heterocycles were effective as inhibitors of both erlotinib-sensitive and erlotinib-resistant cancer cells [15]. Dicationic 2,6-diphenylpyrazines are active against *Trypanosomabruceirhodesiense* (the causative agent of sleeping sickness), and *Plasmodium falciparum* (causative agent of malaria) [16]. Covalent attachment of Ni-2,3-pyrazine dicarboxylic acid onto gold nanoparticle gold electrode modified with penicillamine-CdS quantum dots produced an electrode that can be used for electro catalytic oxidation of urea and determination of some kinetic parameters such as the electron transfer coefficient and the diffusion coefficient of urea [17]. Several pyrazine derivatives were found to possess herbicidal activity and many pyrazinamide derivatives inhibited photosynthetic electron transport in plant chloroplasts [17] and they were found to act as photosystem 2 inhibitors [5]. Pyrazine dicarboxylic acids, as well as their simple carboxylates and amides, can act as multi-dentate ligands in crystal engineering and the construction of binuclear or polynuclear complexes is well established [18,19]. Pyrazinamide (PZA), a first-line antitubercular drug, was discovered through an effort to find anti-tubercular nicotinamide derivatives [20]. Along with rifampicin, PZA is the only clinically used active substance to possess so called sterilizing activity that is the ability to kill the dormant non-growing tubercle bacilli of low metabolism activity. The killing of these persisters is a crucial factor in shortening the therapy course and avoiding relapses. PZA is activated by means of hydrolysis catalyzed by pyrazinamidase to form the active pyrazinoic acid (POA). POA accumulates inside the mycobacterial cell, thus leading to disruption of membrane transport and energetics [21]. POA enters the cell by passive diffusion strongly dependent on pH (greater in acidic conditions). The accumulation also increases in non-growing bacilli, because the POA efflux mechanism is an energy consuming process. Some PZA analogues and derivatives, especially 5-chloropyrazinamide, were also shown to inhibit the FAS I (Fatty Acid Synthase I) pathway, impairing the building of normal mycobacterial cell wall [22]. The title compound of this article, 5-chloro-*N*-(2-fluorophenyl)pyrazine-2-carboxamide, was shown to possess *in vitro* antimycobacterial and inhibited the growth of *M.tuberculosis* with minimal inhibitory concentration of 6.25 µg/Ml [4, 6].

Pyrazine is a widely used model molecule in many theoretical studies because the diazine ring can form different kinds of important compounds or isomers [23, 24]. It is isoelectronic with benzene as it contains 6π electrons for

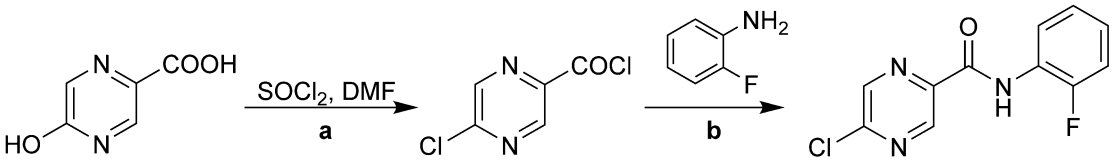

Scheme 1. Preparation of the pyrazine derivative.

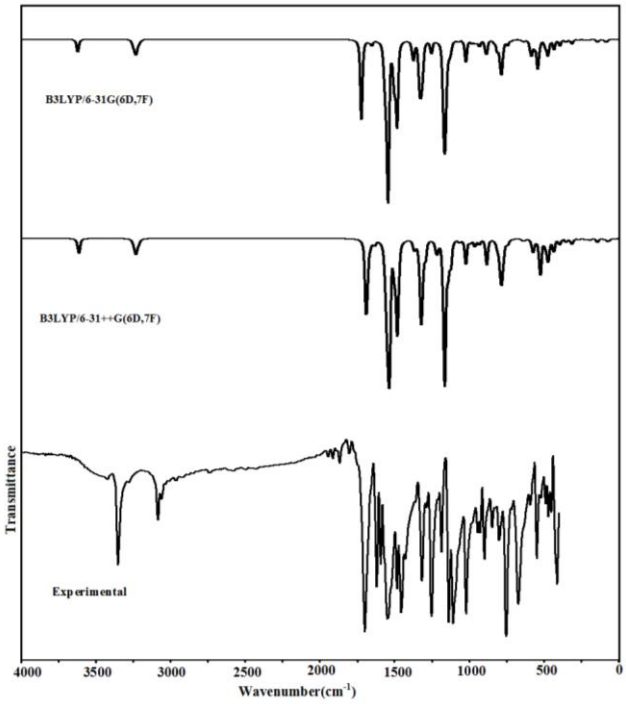

Figure 1. FT-IR spectrum of 5-chloro-*N*-(2-fluorophenyl)pyrazine-2-carboxamide.

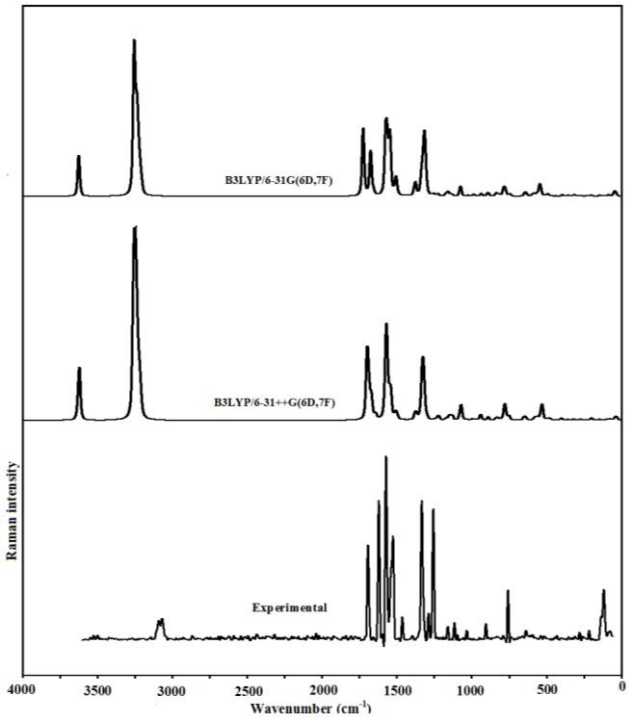

Figure 2. FT-Raman spectrum of 5-chloro-*N*-(2-fluorophenyl)pyrazine-2-carboxamide.

aromatic delocalization. However, the perfect aromaticity of benzene is disturbed by centric substitution of 2 nitrogen atoms in the case of the systems under consideration, such that the electronegative nitrogen hold some of the ring electrons to prevent the perfect delocalization of the 6π electrons. The inclusion of a substituent group in aromatic rings leads to the variation of charge distribution in molecules, and consequently this greatly affects the structural, electronic and vibrational parameters. In general, electron deficient pyrazines undergo electrophilic substitution reactions under normal conditions with the substitution of electron-donating group. That is the pyrazine system becomes more nucleophilic. The vibrational spectroscopic studies of several pyrazine carboxamide derivatives are reported by the authors group [25-27]. Therefore, the vibrational spectroscopic studies of the amides of pyrazine-2-carboxylic acids are added areas of interest. In the present work, FT-IR and FT-Raman spectra of 5-chloro-*N*-(2-fluorophenyl)pyrazine-2-carboxamide are reported both experimentally and theoretically. Also the NBO analysis, molecular electrostatic potential HOMO and LUMO analysis and first hyperpolarizability are also reported. Due to the different potential biological activity of the title compound, molecular docking study is reported.

2. Experimental Details

The pyrazine derivative was prepared as described previously [4, 6] by convenient two-step synthesis using 5-hydroxypyrazine-2-carboxylic acid (5-hydroxy-POA; Sigma Aldrich, Darmstadt, Germany) as a starting material [28]. During the first step 5-hydroxy-POA was treated with thionyl chloride to form 5-chloropyrazine-2-carbonyl chloride (Scheme 1, a) [29]. Dimethylformamide (DMF) was added to the reaction mixture as a catalyst. The title compound 5-chloro-*N*-(2-fluorophenyl)pyrazine-2-carboxamide was prepared by aminolysis of the acyl chloride by 2-fluoroaniline (Scheme 1,b). Reaction proceeded under mild conditions (at RT in acetone), triethylamine (TEA) was used to neutralize the originating HCl. The FT-IR spectrum (Figure 1) was recorded using KBr pellets on a DR/Jasco FT-IR 6300 spectrometer. The FT-Raman spectrum (Figure 2) was obtained on a Bruker RFS 100/s, Germany. For excitation of the spectrum the emission of Nd:YAG laser was used, excitation wavelength 1064 nm, maximal power 150 mW, measurement on solid sample. NMR spectra were recorded on Varian VNMR S500 (Varian, Palo Alto, CA, USA) at 500 MHz for ^{1}H-NMR at ambient temperature in DMSO-*d6*. The chemical shifts as δ values in ppm are indirectly referenced to tetramethylsilane (TMS) *via* the solvent signal.

3. Computational Details

Calculations of the title compound are carried out with Gaussian09 program [30] using the B3LYP/6-31G(6D, 7F) and B3LYP/6-31++G(6D, 7F) basis set to predict the molecular structure and vibrational wavenumbers. Molecular

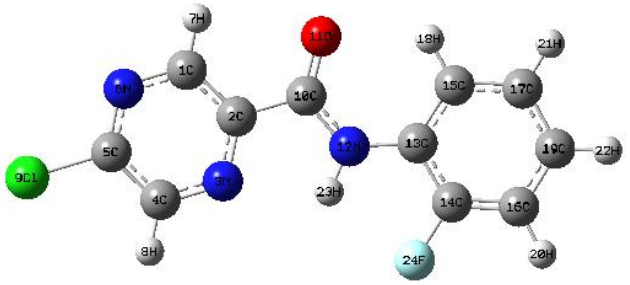

Figure 3. Optimized geometry (B3LYP/6-31++G(6D,7F)) of 5-chloro-*N*-(2-fluorophenyl)pyrazine-2-carboxamide.

geometry was fully optimized by Berny's optimization algorithm using redundant internal coordinates. Harmonic vibrational wavenumbers are calculated using the analytic second derivatives to confirm the convergence to minima on the potential surface. The DFT hybrid B3LYP functional method tended to overestimate the fundamental modes, therefore scaling factor of 0.9613 has to be used for obtaining a considerably better agreement with experimental data [31]. Parameters corresponding to optimized geometry (B3LYP/6-31++G(6D,7F)) of the title compound (Figure 3) are given in Table 1 (see Appendix). The absence of imaginary wavenumbers on the calculated vibrational spectrum confirms that the deducted structure corresponds to minimum energy. The assignments of the calculated wavenumbers are aided by the animation option of GAUSSVIEW program, which gives a visual presentation of the vibrational modes [32]. The potential energy distribution (PED) is calculated with the help of GAR2PED software package [33].

4. Results and Discussion

4.1. IR and Raman Spectra

The observed IR and Raman bands and calculated (scaled) wavenumbers and assignments are given in Table 2 (see Appendix). The phenyl and pyrazine rings are designated as Ph and Pz, respectively.

CCl and CF modes

For simple organic chlorine compounds, C-Cl absorptions are in the region 850-550 cm^{-1}[34]. Renjith et al. [35] reported the C-Cl stretching mode at 644 (IR), 681, 643 (Raman) and at 680, 675, 676, 646 cm^{-1} theoretically and the deformation modes of C-Cl at 353, 339, 266 and 150 cm^{-1}. For the title compound the stretching mode C-Cl is observed in the Raman spectrum at 692 cm^{-1} and at 696 cm^{-1} theoretically. Fluorine atoms directly attached to an aromatic ring give rise to bands in the region 1270-1100 cm^{-1}[36]. The C-F stretching mode is reported at 1233 (IR), 1244 (theoretical) [37] and at 1227 (IR) and 1239 cm^{-1} (theoretical) [38] for fluoro-phenyl compounds. For the title compound the stretching mode υC-F is observed in the Raman spectrum at 1148 cm^{-1}, 1140 cm^{-1} in IR spectrum and at 1153 cm^{-1} theoretically. For the title compound the deformation modes of C-Cl and C-F are assigned at 405, 305, 271 and 483, 444, 267 cm^{-1} theoretically.

C=O modes

The carbonyl group is contained in a large number of different classes of compounds, for which a strong absorption band due to υC=O is observed in the region of 1850-1550 cm^{-1}[39]. The stretching mode of C=O is reported at 1632 (IR), 1616 (Raman) and 1636 cm^{-1} theoretically for a pyrazine-2-carboxamide derivative [25]. The υC=O modes are reported at 1613, 538 cm^{-1} (IR), 1617, 698, 115 cm^{-1} (Raman) and at 1610, 870, 708, 557, 122 cm^{-1} theoretically for carboxamide derivative [40]. For the title compound the band seen at 1585 cm^{-1} in the Raman spectrum, 1593 cm^{-1} in the IR spectrum are assigned as υC=O and theoretically found at 1596 cm^{-1}. In the present case the carbonyl deformation modes are observed at 892, 95 cm^{-1} in the Raman spectrum; 823 cm^{-1} in the IR spectrum and at 875, 832, 88 cm^{-1} theoretically.

NH modes

The N-H stretching vibrations generally give rise to bands at 3500-3300 cm^{-1}[41]. In the present study, the N-H stretching band has split in to a doublet as 3423 and 3352 cm^{-1} in the IR spectrum. The splitting of about 71 cm^{-1} in the IR spectrum is due to strong intramolecular hydrogen bonding between the carboxamide hydrogen (donor) and N_3 pyrazine nitrogen (acceptor). Furthermore, the N-H stretching wavenumber is red-shifted by 46 cm^{-1} in the IR spectrum with a strong intensity from the computed wavenumber, which indicates the weakening of the N-H bond resulting in proton transfer to the neighbouring oxygen atom O_{11} [42]. In *N*-mono-substituted amides, the in-plane bending frequency and the resonance stiffened C-N band stretching frequency fall close together and therefore interact. The C-N-H vibration where the nitrogen and hydrogen move in opposite direction relative to the carbon atom involves both N-H bending mode and C-N stretching and absorbs strongly near 1550 cm^{-1} [36]. This band is very characteristic for mono substituted amides. The C-N-H vibration where the N and H atoms move in the same direction relative to the carbon atom gives rise to a weaker band near 1250 cm^{-1} [36]. In the present case the bands observed at 1530 cm^{-1} in the Raman spectrum 1250 cm^{-1} in the IR spectrum and 1526 and 1245 cm^{-1} (DFT) are assigned as C-N-H bending modes.The N-H out of plane mode is expected in the range 735 ± 60 cm^{-1} [43]. The N-H out-of-plane deformation of the title compound is observed at 823 cm^{-1} in the IR spectrum and at 832 cm^{-1} theoretically which is in good agreement with similar derivatives [44].

Phenyl ring modes

According to Roeges [45] the C-H stretching vibrations of the 1,2-disubstituted benzene are expected in the region 3120-3000 cm^{-1}. In the present case phenyl C-H stretching modes are observed at 3085 cm^{-1} in the IR spectrum, 3113, 3076 cm^{-1} in the Raman spectrum and at 3149, 3117, 3101 and 3085 cm^{-1} theoretically. The benzene ring possesses six ring stretching vibrations, of which the four with the highest frequencies (occurring respectively near 1600, 1580, 1490, and 1440 cm^{-1}) are good group vibrations [45]. The fifth ring stretching vibration is active near 1315 ± 65 cm^{-1}, a region that overlaps strongly with that of the C-H in-plane deformation. The sixth ring stretching vibration or ring breathing mode appears as a weak band near 1000 cm^{-1} in mono and 1,3-di- and 1,3,5-tri-substituted benzenes. In the otherwise substituted benzenes, however, this vibration is substituent sensitive [45]. The ring stretching vibration υPh modes are expected in the region 1615-1260 cm^{-1}. For the title compound υPh modes are observed at 1620, 1571, 1454 and 1320 cm^{-1} in the IR spectrum and 1603, 1575, 1474, 1447 and 1346 cm^{-1} in the Raman spectrum. The DFT calculation gives modes at 1610, 1576, 1468, 1444 and 1333 cm^{-1}. In ortho-di-

substitution the ring breathing mode [46] has three frequency intervals according to whether both substituent are heavy, or one of them is heavy while the other is light or both of them are light. In the first case, the interval is 1100-1130 cm^{-1}, in the second case it is 1020-1070 cm^{-1}, while in the third case it is between 630 and 789 cm^{-1}. In the present case the band observed at 1021 cm^{-1} in the IR spectrum, 1019 cm^{-1} in the Raman spectrum and 1023 cm^{-1} in the DFT calculation is confirmed as the ring breathing mode of the phenyl ring. Kaur et al. [47] reported the ring breathing mode of ortho substituted benzene rings at 1026 and 1023 cm^{-1} theoretically. The C-H in-plane deformation of 1,2-disubstituted benzene is expected in the range 1280-1000 cm^{-1} [45]. For the title compound the phenyl C-H in-plane deformation δCHPh are observed at 1140, and 1066 cm^{-1} in the IR spectrum and at 1270, 1167 and 1148 cm^{-1} in the Raman spectrum. The DFT calculation gives δCHPh mode at 1271, 1170, 1153 and 1074 cm^{-1}. The aromatic C-H out-of-plane deformations [45] are expected in the range 990-740 cm^{-1}. These γCHPh modes are observed at 993, 945, 754 cm^{-1} in the IR spectrum, 857, 764 cm^{-1} in the Raman spectrum and corresponding calculated values are 994, 953, 872, 760 cm^{-1}. The in-plane and out-of-plane deformation modes of the phenyl ring are also identified and assigned (Table 2) (see Appendix).

Pyrazine ring modes

For the title compound, the pyrazine ring stretching modes υPz are observed at 1509, 1238 and 1191 cm^{-1} in the Raman spectrum; 1515, 1483, 1288 and 1187 cm^{-1} in the IR spectrum and calculated values are 1514, 1491, 1291, 1240 and 1195 cm^{-1}. The ring breathing mode of the pyrazine ring is observed at 1090 cm^{-1} in the IR spectrum, 1082 cm^{-1} in the Raman spectrum and at 1089 cm^{-1} theoretically. The ring breathing mode of pyrazine is reported at 1015 cm^{-1} [40]. In the Raman spectrum of 2,6-dichloropyrazine and 2-chloropyrazine the ring breathing mode is reported at 1131 and 1049 cm^{-1} [48]. For a pyrazine carboxamide derivative, the pyrazine ring stretching modes are observed at 1533, 1475 and 1416 cm^{-1} in the IR spectrum, 1528, 1417, 1188 and 1000 cm^{-1} in the Raman spectrum and 1526, 1489, 1424, 1183, 1002 and 977 cm^{-1} theoretically [25]. For similar pyrazine-2-carboxamide derivatives the pyrazine ring stretching modes are observed at 1523, 1291 cm^{-1} in the Raman spectrum, 1531, 1293, 1213, 1162 cm^{-1} in the IR spectrum and at 1527, 1481, 1291, 1207, 1177 cm^{-1} theoretically and 1533, 1475, 1416 cm^{-1} (IR); 1528, 1417, 1188, 1000 cm^{-1} (Raman) and at 1526, 1489, 1424, 1183, 1002 and 977 cm^{-1} in theoretical calculation [40]. The C-H stretching modes of pyrazine were reported in the range 3100-3000 cm^{-1} [48, 49]. These υC-H bands are observed at 3057, 3070 and 3086 cm^{-1} (IR); 3060, 3070 and 3087 cm^{-1} (Raman); and 3061, 3074 and 3079 cm^{-1} (theoretical) for 2-chloropyrazine; and at 3099 and 3104 cm^{-1}(IR); 3078 and 3103 cm^{-1} (Raman); and 3096, 3100 cm^{-1} (calculated) for 2,6-dichloropyrazine [48]. For the title compound the υCHPz modes are observed at 3130 cm^{-1} in the Raman spectrum and the calculated values at 3143 and 3126 cm^{-1}. The C-H in-plane bending modes in 2,6-dichloropyrazine are reported at 1189 and 1151 cm^{-1} in the IR spectrum [48]. For 2-chloropyrazine these modes are reported at 1455, 1380, 1280, and 1179 cm^{-1} in the IR spectrum and at 1457, 1390, 1289, and 1167 cm^{-1} theoretically [48]. For pyrazine the δC-H modes are observed at 1485, 1413 and 1065 cm^{-1} in the IR spectrum and at 1482, 1412, 1227 and 1063 cm^{-1} theoretically [48] and for pyrazinamide [50] the bands are at 1305, 1183 and 1054 cm^{-1} (theoretical). In the present case CHPz in-plane deformation is observed at 1405 and 1301 cm^{-1} in Raman spectrum; at 1422 cm^{-1} in IR spectrum ; at 1297and 1417 cm^{-1} theoretically. For pyrazine γC-H modes are observed at 790 cm^{-1} in the IR spectrum, 976 and 925 cm^{-1} in the Raman spectrum, and at 985, 974, 930 and 790 cm^{-1} by DFT calculations [48]. The γC-H modes are reported at 954, 929 and 844 cm^{-1} (IR); 960, 928 and 847 cm^{-1} (Raman); and 960, 923 and 837 cm^{-1} (theoretical) for 2-chloropyrazine; and at 897 and 875 cm^{-1} (IR); 896 cm^{-1} (Raman); and 919 and 869 cm^{-1} theoretically for 2,6-dichloropyrazine [48]. For 2-aminopyrazine-3-carboxylic acid γC-H modes are reported at 1006 and 850 cm^{-1} in the Raman spectrum, 987 and 852 cm^{-1} by HF calculations, and at 988, 954 and 786 cm^{-1} for pyrazinamide [51]. For the title compound the CHPz out-of-plane deformation is observed at 957 and 914 cm^{-1} in Raman spectrum; 926 cm^{-1} in the IR spectrum ; at 954 and 915 cm^{-1} theoretically. Most of the vibrations are not pure but contains significant contribution from other modes.

In order to investigate the performance of vibrational wavenumbers of the title compound, the root mean square (RMS) value between the calculated and observed wavenumbers were calculated. The RMS values of wavenumbers were calculated using the following expression [52].

$$RMS = \sqrt{\frac{1}{n-1}\sum_i^n (vi^{calc} - vi^{exp})^2}$$

The RMS error of the observed IR and Raman bands are found to be 15.12 and 21.91 for B3LYP/6-31G(6D, 7F) and 7.80 and 9.24 for B3LYP/6-31++G(6D, 7F) method. The small differences between experimental and calculated vibrational modes are observed. This is due to the fact that experimental results belong to solid phase and theoretical calculations belong to gaseous phase.

4.2. Geometrical parameters

In the present case the pyrazine bond lengths of C_1-C_2, C_2-N_3, N_3-C_4, C_4-C_5, C_5-N_6 and N_6-C_1 are 1.4004, 1.3572, 1.3431, 1.4032, 1.3245 and 1.3357Å respectively. For similar derivatives, Mary et al. [44] reported the corresponding values as 1.3840, 1.3229, 1.2996, 1.3917, 1.3116 and 1.3220Å. For a similar pyrazine derivative, Bhagyasree et al. reported the corresponding values are 1.406, 1.358, 1.326, 1.437, 1.360 and 1.354Å respectively [27]. For 3-aminopyrazine-2-carboxylic acid [48] and for a similar substituted amide of pyrazine [44] the bond length of C_{10}-O_{11}, C_2-C_{10}, C_2-N_3 and C_2-C_1 are 1.21, 1.479, 1.333 and 1.479Å and 1.2003, 1.5099, 1.3229 and 1.479Å respectively. In the present case the corresponding values are 1.2423, 1.5004, 1.3572 and 1.4004Å. The C-N bond lengths in the pyrazine ring of the title compound C_2-N_3, C_4-N_3, C_5-N_6 and C_1-N_6 are 1.3572, 1.3431, 1.3245 and 1.3557Å are much shorter than the normal C-N single bond that is referred to 1.49Å. The same results are shown for the bond length of the C-C bonds, C_1-C_2 1.4004Å and C_4-C_5 1.4032Å in the pyrazine ring and are also smaller than that of the normal bond of 1.54Å [53]. The C-N bond lengths C_{10}-N_{12} and C_{13}-N_{12} are 1.3827 and 1.4260Å are also shorter than the normal C-N single bond of 1.49Å, which confirms this bonds to have some character of a double or conjugated bond [53. The C-Cl bond length in the present case is 1.8106Å which is in good

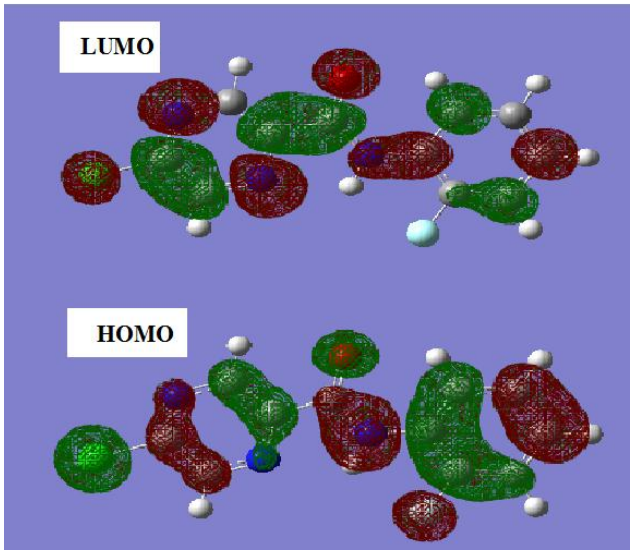

Figure 4. HOMO and LUMO plots of 5-chloro-*N*-(2-fluorophenyl)pyrazine-2-carboxamide.

agreement with the previous reported values [44, 48]. The substitution of chlorine in the pyrazine ring shortens the C_5-N_6 bond length and elongates C_5-C_4 bond length, in comparison with the other C-N and C-C bond lengths of the pyrazine ring. Chlorine is highly electronegative and tries to obtain additional electron density. It attempts to draw it from the neighbouring atoms, which moves closer together in order to share the remaining electrons more easily as a result. Due to this the bond angle C_5-C_4-N_3 is found to be 120.1˚ and the exocyclic angles C_4-C_5-Cl_9 and N_6-C_5-Cl_9 become 119.3 and 117.8˚ respectively. The C-F bond lengths are reported as1.4068, 1.3284, 1.3251, 1.3284Å theoretically [54]. For *N*-[(4-trifluoromethyl)phenyl]pyrazine-2-carboxamide the C-F bond length are in the range 1.4025-1.4163Å [55]. For the title compound C_{14}-F_{24} bond length is 1.4002Å. At N_{12} position, the angles C_{10}-N_{12}-H_{23} is 118.9˚, C_{13}-N_{12}-H_{23} is 117.7˚and C_{10}-N_{12}-C_{13} is 123.2˚. This asymmetry of the angles at N_{12} position indicates the weakening of N_{12}-H_{23} bond resulting in proton transfer to the oxygen atom O_{11} [56, 57]. All the carbon–carbon bond lengths in the phenyl ring lies in the range 1.3884-1.4029Å and C-H bond lengths in the range 1.0834-1.0854Å. Thus the theoretical results obtained are almost comparable with the reported structural parameters of similar molecules.

4.3. Frontier molecular orbitals

To explain several types of reactions and for predicting the most reactive position in conjugated systems, molecular orbitals and their properties such as energy is used [58]. The highest occupied molecular orbital (HOMO) and lowest unoccupied molecular orbital (LUMO) are the most important orbitals in a molecule. The eigen values of HOMO and LUMO and their energy gap reflect the biological activity of the molecule. A molecule having a small frontier orbitals gap is more polarizable and is generally associated with a high chemical reactivity and low kinetic stability [59, 60]. HOMO, which can be thought as the outer orbital containing electrons, tends to give these electrons as an electron donor and hence the ionization potential is directly related to the energy of the HOMO. On the other hand LUMO can accept electrons and the LUMO energy is directly related to electron affinity [61]. HOMO and LUMO were examined for the title compound as given in Figure 4. For understanding various aspects of pharmacological sciences including drug design and the possible ecotoxicological characteristics of the drug molecules, several new chemical reactivity descriptors have been proposed. Conceptual DFT based descriptors have helped in many ways to understand the structure of molecules and their reactivity by calculating the chemical potential, global hardness and electrophilicity. Using HOMO and LUMO orbital energies, the ionization energy (I) and electron affinity (A) can be expressed as: $I = -E_{HOMO}$, $A = -E_{LUMO}$. The global hardness η and chemical potential μ are given by the following relation $\eta = (I-A)/2$ and $\mu = -(I+A)/2$. Parr et al. [62] proposed the global electrophilicity power of a ligand $\omega = \mu^2/2\eta$. This index measures the stabilization in energy when the system acquires an additional electronic charge from the environment. Electrophilicity encompasses both the ability of an electrophile to acquire additional electronic charge and the resistance of the system to exchange electronic charge with the environment. It contains information about both electron transfer (chemical potential, μ) and stability (hardness, η) and is a better descriptor of global chemical reactivity. For the title compound the descriptors were calculated as follows: ionisation potential I = 8.5397 eV, electron affinity A = 5.3577 eV, global hardness η = 1.591 eV, chemical potential μ = -6.9487 eV, and global electrophilicity ω = 15.1742 eV. It is seen that the chemical potential of the title compound is negative and it means that the compound is stable. It does not decompose spontaneously in the elements it is made up of. The hardness signifies the resistance toward the deformation of electron cloud of chemical systems under small perturbation encountered during the chemical process. The principle of hardness works in Chemistry and Physics but it is not physically observable. Soft systems are large and highly polarisable, while hard systems are relatively small and much less polarisable.

4.4. Molecular electrostatic potential (MEP)

MEP is related to the electron density (ED) and is a very useful descriptor in understanding sites for electrophilic and nucleophilic reactions as well as hydrogen bonding interactions [63, 64]. The electrostatic potential V(r) is also well suited for analysing processes based on the ‘‘recognition’’ of one molecule by another, as in drug-receptor, and enzyme-substrate interactions, because it is through their potentials that the two species first ‘‘see’’ each other [65, 66]. To predict reactive sites for electrophilic and nucleophilic attacks for the investigated molecule, MEP at the B3LYP/6-31++G (6D, 7F) optimized geometry was calculated. The different values of the electrostatic potential at the MEP surface are represented by different colours: red, blue and green represent the regions of most negative, most positive and zero electrostatic potential respectively. The negative electrostatic potential corresponds to an attraction of the proton by the aggregate electron density in the molecule (shades of red), while the positive electrostatic potential corresponds to the repulsion of the proton by the atomic nuclei (shade of blue). The negative (red and yellow) regions of MEP were related to electrophilic reactivity and the positive (blue) regions to nucleophilic reactivity (Figure 5). From the MEP it is evident that the negative charge covers the C=O group and the positive region is over the NH group. The value of the electrostatic potential is largely responsible for the binding of a substrate to its receptor binding sites since the

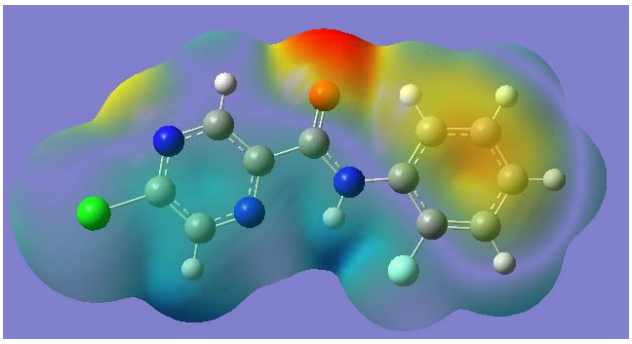

Figure 5. MEP plot of 5-chloro-*N*-(2-fluorophenyl)pyrazine-2-carboxamide.

receptor and the corresponding ligands recognize each other at their molecular surface [67].

4.5. Natural bond orbital analysis

The natural bond orbitals (NBO) calculations were performed using NBO 3.1 program [68] as implemented in the Gaussian09 package at the DFT/B3LYP level in order to understand various second-order interactions between the filled orbitals of one subsystem and vacant orbitals of another subsystem, which is a measure of the intermolecular delocalization or hyper conjugation. NBO analysis provides the most accurate possible 'natural Lewis structure' picture of 'j' because all orbital details are mathematically chosen to include the highest possible percentage of the electron density. A useful aspect of the NBO method is that it gives information about interactions of both filled and virtual orbital spaces that could enhance the analysis of intra and inter molecular interactions. The second-order Fock-matrix was carried out to evaluate the donor-acceptor interactions in the NBO basis. The interactions result in a loss of occupancy from the localized NBO of the idealized Lewis structure into an empty non-Lewis orbital. For each donor (i) and acceptor (j) the stabilization energy (E(2)) associated with the delocalization i→j is determined as

$$E(2) = \Delta E_{ij} = q_i \frac{(F_{ij})^2}{(E_j - E_i)}$$

qi is donor orbital occupancy, E_i, E_j are the diagonal elements, and F_{ij} is the off diagonal NBO Fock- matrix element.

In NBO analysis large E (2) value shows the intensive interaction between electron-donors and electron-acceptors, and greater the extent of conjugation of the whole system, the possible intensive interaction are given in Table 3 (see Appendix). The second-order perturbation theory analysis of Fock-matrix in NBO basis shows strong intra-molecular hyper conjugative interactions are formed by orbital overlap between n(Cl), n(O), n(N), n(F) and σ*(C-C), π*(C-N), σ*(C-N), π*(C-O), π*(C-C) bond orbitals which result in intra-molecular charge transfer (ICT) causing stabilization of the system. These interactions are observed as an increase in electron density (ED) in N-C, C-O and C-C anti bonding orbital that weakens the respective bonds. We observed a strong intra-molecular hyper conjugative interaction of C_4-C_5 from N_3 of n_1 (N_3)→σ*(C_4-C_5) which increases ED (0.04565 e) and weakens the respective bonds C_4-C_5 leading to stabilization of 9.72 kJ/mol and also the hyper conjugative interaction of C_4-C_5 from N_6 of n_1 (N_6)→σ*(C_4-C_5) which increases ED (0.04565 e) and weakens the respective bonds C_4-C_5 leading to stabilization of 9.78 kJ/mol. Another strong intra-molecular hyper conjugative interaction of C_5-N_6 from Cl_9 of n_3 (Cl_9)→π*(C_5-N_6) which increases ED (0.39212e) and weakens the respective bonds C_5-N_6 leading to stabilization of 13.23 kJ/mol and also the hyper conjugative interaction of C_{10}-N_{12} from O_{11} of n_2 (O_{11})→σ*(C_{10}-N_{12}) which increases ED (0.08281e) and weakens the respective bonds C_{10}-N_{12} leading to stabilization of 25.83 kJ/mol. There occurs a strong intra-molecular hyper conjugative interaction of C_{10}-O_{11} from N_{12} of n_1 (N_{12})→π*(C_{10}-O_{11}) which increases ED (0.25912e) and weakens the respective bonds C_{10}-O_{11} leading to stabilization of 44.07 kJ/mol and also the hyper conjugative interaction of C_{14}-C_{16} from F_{24} of n_3 (F_{24})→σ*(C_{14}-C_{16}) which increases ED (0.36172e) and weakens the respective bonds C_{14}-C_{16} leading to stabilization of 17.62 kJ/mol.

The NBO analysis describes the bonding in terms of the natural hybrid orbital n_3 (Cl_9), which occupies a higher energy orbital (-0.32940 a.u) with considerable p-character (100 %) and low occupation number (1.92371) and the other n_1 (Cl_9) orbital, which occupies a lower energy orbital (-0.92782 a.u.) with p-character (15.04 %) and high occupation number (1.99480). The NBO analysis also describes the bonding in terms of the natural hybrid orbital n_2 (O_{11}), which occupies a higher energy orbital (-0.24503 a.u) with considerable p-character (99.99 %) and low occupation number (1.85716) and the other n_1 (O_{11}) orbital, which occupies a lower energy orbital (-0.68834 a.u) with p-character (38.98 %) and high occupation number (1.97848). The NBO analysis also describes the bonding in terms of the natural hybrid orbital n_3 (F_{24}), which occupies a higher energy orbital (-0.39494 a.u) with considerable p-character (99.99 %) and low occupation number (1.92224) and the other n_1 (F_{24}) orbital, which occupies a lower energy orbital (-0.04259a.u) with p-character (27.49 %) and high occupation number (1.98953). Thus, a very close to pure p-type lone pair orbital participates in the electron donation to the σ*(C_4-C_5) orbital for n_1 (N_3)→σ*(C_4-C_5), σ*(C_4-C_5) orbital for n_1 (N_6)→σ*(C_4-C_5), π*(C_5-N_6) orbital for n_3 (Cl_9)→π*(C_5-N_6), σ* (C_{10}-N_{12}) orbital for n_2 (O_{11})→σ*(C_{10}-N_{12}), π*(C_{10}-O_{11}) orbital for n_1 (N_{12})→π*(C_{10}-O_{11}) and π*(C_{14}-C_{16}) orbital for n_3 (F_{24})→π*(C_{14}-C_{16}) interaction in the compound. The results are tabulated in Table 4 (see Appendix).

4.6. Nonlinear optical properties

Nonlinear optics (NLO) deals with the interaction of applied electromagnetic fields with various materials to generate new electromagnetic fields, altered in wavenumber, phase, or other physical properties [69]. Organic molecules able to manipulate photonic signals efficiently are of importance in technologies such as optical communication, optical computing, and dynamic image processing [70, 71]. In this context, the dynamic first hyperpolarizability of the title compound is also calculated in the present study. The first hyperpolarizability (β_0) of this novel molecular system is calculated using B3LYP/6-31++G (6D, 7F) method, based on the finite field approach. In the presence of an applied electric field, the energy of a system is a function of the electric field. First hyperpolarizability is a third rank tensor that can be described by a 3 × 3 × 3 matrix. The 27 components of the 3D matrix can be reduced to 10 components due to the Kleinman symmetry [72]. The components of β are defined as the coefficients in the Taylor series expansion of the energy in the

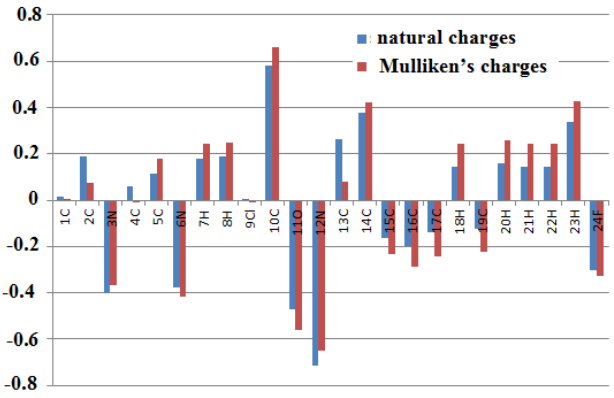

Figure 6. Comparative graph of Mullikens and natural atomic charges of 5-chloro-*N*-(2-fluorophenyl)pyrazine-2-carboxamide.

external electric field. When the electric field is weak and homogeneous, this expansion becomes

$$E = E_0 - \sum_i \mu_i F^i - \frac{1}{2}\sum_{ij} \alpha_{ij} F^i F^j - \frac{1}{6}\sum_{ijk} \beta_{ijk} F^i F^j F^k - \frac{1}{24}\sum_{ijkl} \gamma_{ijkl} F^i F^j F^k F^l + \cdots$$

where E_0 is the energy of the unperturbed molecule, F^i is the field at the origin, μ_i, α_{ij}, β_{ijk} and γ_{ijkl} are the components of dipole moment, polarizability, the first hyperpolarizabilities, and second hyperpolarizabilities respectively. The calculated first hyperpolarizability of the title compound is 1.3890 $\times 10^{-30}$ e.s.u. which is 11 times that of standard NLO material urea (0.13 $\times 10^{-30}$ e.s.u.) [73]. The reported values of hyperpolarizability of similar derivatives are 1.004884 $\times$ 10^{-30} e.s.u. [74]. The second hyperpolarizability is calculated using the using the following formula:

$$\gamma_{ijkl} = \frac{1}{5}(\gamma_{xxxx} + \gamma_{yyyy} + \gamma_{zzzz} + 2\gamma_{xxyy} + 2\gamma_{yyzz} + 2\gamma_{xxzz})$$

The second hyperpolarizability of the title compound is -0.1464×10^{-35}e.s.u. [75]. Thus the present material has a reasonably good propensity for nonlinear optical activity.

4.7. Mulliken charges

The calculation of atomic charges plays an important role in the application of quantum mechanical calculations to molecular systems. Mulliken charges are calculated by determining the electron population of each atom as defined in the basis functions. The charge distributions calculated by the Mulliken [76] and NBO methods for the equilibrium geometry of 5-chloro-*N*-(2-fluorophenyl)pyrazine-2-carboxamide are given in Table 5 (see Appendix). The charge distribution in the molecule has an important influence on the vibrational spectra. In the title compound the Mulliken atomic charge of the carbon atoms in the neighbourhood of C_2, C_5, C_{10}, C_{13} and C_{14} are more positive shows the direction of delocalization while C_4 natural atomic charges give negative value shows that the natural atomic charges are more sensitive to the changes in the molecular structure than Mulliken net charge. Also we have done a comparison of Mulliken charge (Figure 6) obtained by different basis sets to assess the sensitivity of the calculated charges to changes in the basis set and quantum mechanical method and tabulated in the Table 6 (see Appendix).

4.8. ^{1}H NMR spectrum

With TMS as internal standard, experimental spectrum data of 5-chloro-*N*-(2-fluorophenyl)pyrazine-2-carboxamide in DMSO is obtained at 500 MHz and is shown in Table 7 (see Appendix). B3LYP/GIAO was used to calculate the absolute isotropic chemical shielding of 5-chloro-*N*-(2-fluorophenyl)pyrazine-2-carboxamide [77]. Relative chemical shifts were then estimated by using the corresponding TMS shielding: σ_{calc} (TMS) calculated in advance at the same theoretical level as this paper. Numerical values of chemical shift $\delta_{pred} = \sigma_{calc}$ (TMS) -σ_{calc} together with calculated values of σ_{calc} (TMS), are reported in Table 7 (see Appendix). It is seen that chemical shift was in agreement with the experimental ^{1}H NMR data. Thus, the results have shown that the predicted proton chemical shifts were in good agreement with the experimental data for 5-chloro-*N*-(2-fluorophenyl)pyrazine-2-carboxamide.

4.9. Molecular docking

It is evident from the literature that pyrazine derivatives have shown promising antimicrobial activity [78, 79]. Enoyl-acyl carrier protein (ACP) reductase is a key enzyme of the type II fatty acid synthases system. ACP reductase being a well-established target for antimicrobial drugs [80, 81] was therefore selected as the target macromolecule for docking simulations. High resolution crystal structure of ACP reductase was downloaded from the RCSB PDB website (PDB ID: 1QG6) [82]. All molecular docking calculations were performed on AutoDock-Vina software [83]. The protein was prepared for docking by removing the co-crystallized ligands, waters and co-factors. The AutoDockTools (ADT) graphical user interface was used to calculate Kollman charges and polar hydrogens. The ligand was prepared for docking by minimizing its energy at B3LYP/6-31++G (6D, 7F) level of theory. Partial charges were calculated by Geistenger method. The active site of the enzyme was defined to include residues of the active site within the grid size of 40Å×40Å×40Å. The most popular algorithm, Lamarckian Genetic Algorithm (LGA) available in Autodock was employed for docking. The docking protocol was tested by extracting co-crystallized inhibitor from the protein and then docking the same. The docking protocol predicted the same conformation as was present in the crystal structure with RMSD value well within the reliable range of 2Å. Amongst the docked conformations, one which bound well at the active site was analyzed for detailed interactions in Discover Studio Visualizer 4.0 software. The ligand binds at the active site (Figures 7 and 8) by weak non-covalent interactions. Thr194 and Ile192 form *H*-bonds with the docked ligand. The docked ligand 5-chloro-*N*-(2-fluorophenyl)pyrazine-2-carboxamide forms a stable complex with ACP reductase and gives a binding affinity (ΔG in kcal/mol) value of -7.4 (Table 8) (see Appendix). These preliminary results suggest that the compound might exhibit inhibitory activity against ACP reductase. However biological tests need to be done to validate the computational predictions.

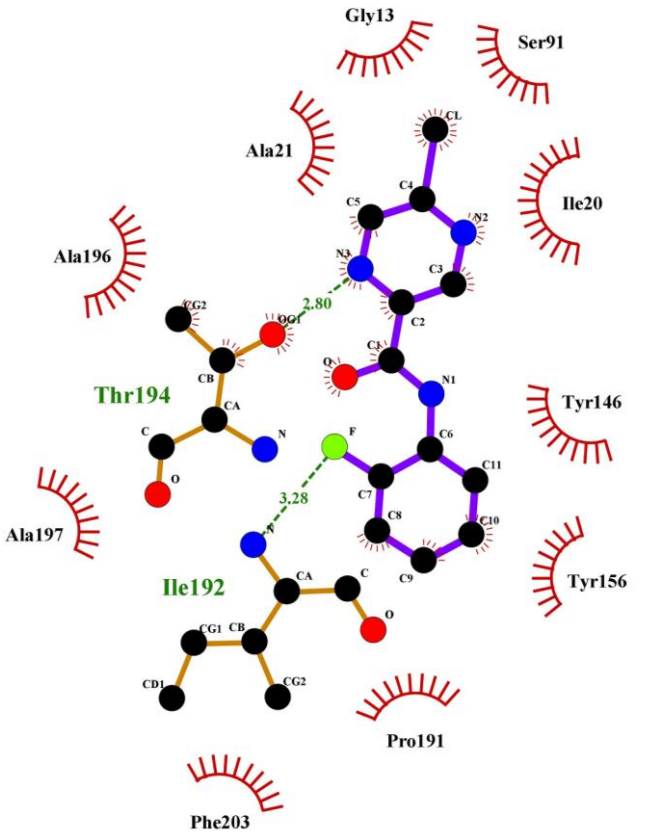

Figure 7. Schematic for the docked conformation of 5-chloro-*N*-(2-fluorophenyl)pyrazine-2-carboxamide at the active site of ACP reductase.

5. Conclusions

The vibrational spectroscopic studies of 5-chloro-*N*-(2-fluorophenyl)pyrazine-2-carboxamide in the ground state were reported experimentally and theoretically. Potential energy distribution of normal modes of vibrations was done using GAR2PED program. The ring stretching modes in IR and Raman spectra are evidence for charge transfer interaction between the donor and the acceptor group through the π system. This along with the lowering of HOMO-LUMO band gap supports for the bioactivity of the molecule. NBO analysis predicts a strong intra-molecular hyper conjugative interaction of ($C_4 \rightarrow C_5$) from N_3 and N_6 of n_1 (N_3) and n_1 (N_6), ($C_5 \rightarrow N_6$) fromCl_9 of n_3(Cl_9), ($C_{10} \rightarrow N_{12}$) from O_{11} of n_2 (O_{11}), ($C_{10} \rightarrow O_{11}$) from N_{12} of n_1 (N_{12}) and ($C_{14} \rightarrow C_{16}$) from F_{24} of n_3 (F_{24}). MEP predicts the most reactive part in the molecule. The calculated first hyperpolarizability of the title compound is comparable with the reported values of similar derivatives and makes it an attractive object for future studies in nonlinear optics. The title compound, 5-chloro-N-(2-fluorophenyl)pyrazine-2-carboxamide forms a stable complex with ACP reductase and gives a binding affinity (ΔG in kcal/mol) value of -7.4 and results suggest that the compound might exhibit inhibitory activity against ACP reductase.

Acknowledgements

The authors are thankful to University of Antwerp for access to the University's CalcUA supercomputer cluster. K. S. Resmi would like to thank University of Kerala, India for a research fellowship.

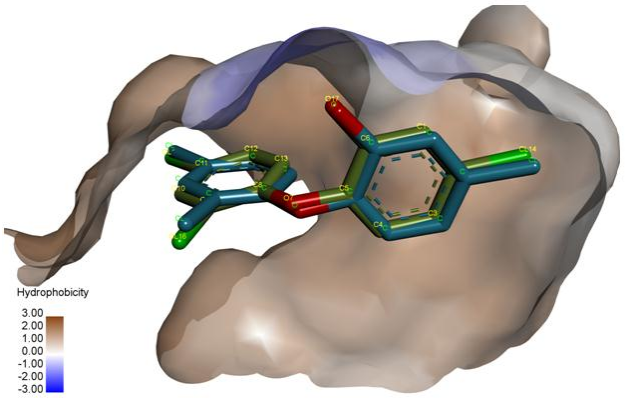

Figure 8. The docked protocol reproduced the co-crystallized conformation (green) with MSD value close to zero confirming the accuracy of the docking protocol.

References

1. H. H. Chen, A. Namil, B. Severns, J. Ward, C. Kelly, C. Drace, M. A. McLaughlin, S. Yacoub, B. Li, R. Patil, N. Sharif, M. R. Hellberg, A. Rusinko, I. H. Pang, K. D. Combrink, Bioorg. Med. Chem. Lett. 24 (2014) 1875–1879.
2. A. R. Farghaly, S. Esmail, A. Abdel-Zahar, A. Abdel-Hafez, H. El-Kashef, Bioorg. Med. Chem. 22 (2014) 2166.
3. M. Hamada, V. Roy, T. R. McBrayer, T. Whitaker, C. Urbina-Blanco, S. P. Nolan, J. Balzarini, R. Snoeck, G. Andrei, R. F. Schinazi, L. A. Agrofoglio, Eur. J. Med. Chem. 67 (2013) 398.
4. B. Servusova, J. Vobickova, P. Paterova, V. Kubicek, J. Kunes, M. Dolezal, J. Zitko, Bioorg. Med. Chem. Lett. 23 (2013) 3589–3591.
5. M. Dolezal, P. Cmedlova, L. Palek, J. Vinsova, J. Kunes, V. Buchta, J. Jampilek, K. Kralova, Eur. J. Med. Chem. 43 (2008) 1105.
6. J. Zitko, B. Servusova, P. Paterova, J. Mandikova, V. Kubicek, R. Kucera, V. Hrabcova, J. Kunes, O. Soukup, M. Dolezal, Molecules 18 (2013) 14807.
7. T. I. El-Emary, J. Chin. Chem. Soc. 53 (2006) 391.
8. J. M. Cox, B. Harper, A. Mastracchio, B. Leiting, R. Sinha Roy, R. A. Patel, J. K. Wu, K. A. Lyons, H. He, S. Xu, B. Zhu, N. A. Thornberry, A. E. Webera, S. D. Edmondson, Bioorg. Med. Chem. Lett. 17 (2007) 4579.
9. C. A. Blum, T. Caldwell, X. Zheng, R. Bakthavatchalam, S. Capitosti, H. Brielmann, S. D. Lombaert, M. T. Kershaw, D. Matson, J. E. Krause, D. Cortright, M. Crandall, W. J. Martin, B. A. Murphy, S. Boyce, A. B. Jones, G. Mason, W. Rycroft, H. Perrett, R. Conley, N. B. Davies, B. L. Chenard, K. J. Hodgetts, J. Med. Chem. 53 (2010) 3330.
10. P. Forns, C. Esteve, L. Taboada, J. A. Alonso, A. Orellana, M. Maldonado, C. Carreno, I. Ramis, M. Lopez, M. Miralpeix, B. Vidal, Bioorg. Med. Chem. Lett. 22 (2012) 2784.
11. Z. Shiokawa, K. Hashimoto, B. Saito, Y. Oguro, H. Sumi, M. Yabuki, M. Yoshimatsu, Y. Kosugi, Y. Debori, N. Morishita, D. R. Dougan, G. P. Snell, S. Yoshida, T. Ishikawa, Bioorg. Med. Chem. 21 (2013) 7938–7954.
12. V. T. Yilmaz, E. Senel, E. Guney, C. Kazak, Inorg. Chem. Commun. 11 (2008) 1330.
13. J. W. Leahy, C. A. Buhr, H. W. B. Johnson, B. Gyu Kim, T. G. Baik, J. Cannoy, T. P. Forsyth, J. W. Jeong, M. S. Lee, S. Ma, K. Noson, L. Wang, M. Williams, J. M. Nuss, E. Brooks, P. Foster, L. Goon, N. Heald, C. Holst, C. Jaeger, S. Lam, J. Lougheed, L. Nguyen, A. Plonowski, J. Song, T. Stout, X. Wu, M. F. Yakes, P. Yu, W. Zhang, P. Lamb, O. Raeber, J. Med. Chem. 55 (2012) 5467.
14. F. Zhang, Q. Wen, S. F. Wang, B. S. Karim, Y. S. Yang, J. J. Liu, W. M. Zhang, H. L. Zhu, Bioorg. Med. Chem. Lett. 24 (2014) 90–95.

15. L. Kekesi, A. Sipos, G. Nemeth, J. Pato, N. Breza, F. Baska, L. Orfi, G. Keri, Bioorg. Med. Chem. Lett. 23 (2013) 6152–6155.
16. L. Hu, A. Patel, L. Bondada, S. Yang, M. Z. Wang, M. Munde, W. D. Wilson, T. Wenzler, R. Brun, D. W. Boykin, Bioorg. Med. Chem. 21 (2013) 6732–6741.
17. A. Azadbakht, M. B. Gholivand, Electrochim. Acta 125 (2014) 9–21.
18. P. C. R. Soares-Santos, L. Cunha-Silva, F. A. A. Paz, R. A. S. Ferreira, J. Rocha, L. D. Carlos, H. I. S. Nogueira, Inorg. Chem. 49 (2010) 3428–3440.
19. X. M. Lin, L. Chen, H. C. Fang, Z. Y. Zhou, X. X. Zhou, J. Q. Chen, A. W. Xu, Y. P. Cai, Inorg. Chim. Acta 362 (2009) 2619–2626.
20. M. Dolezal, Chem. Listy 100 (2006) 959–966.
21. Y. Zhang, M. M. Wade, A. Scorpio, H. Zhang, Z. J. Sun, J. Antimicrob. Chemother. 52 (2003) 790.
22. S. C. Ngo, O. Zimhony, W. J. Chung, H. Sayahi, W. R., Jr. Jacobs, J. T. Welch, Antimicrob. Agents Chemother. 51 (2007) 2430.
23. L. Cui, Z. Liu, S. Duan, D. Y. Wu, B. Ren, Z. Q. Tian, S. Z. Zou, J. Phys. Chem. B 109 (2005) 17597.
24. A. D. Boese, J. M. L. Martin, J. Phys. Chem. A 108 (2004) 3085.
25. T. Joseph, H.T. Varghese, C.Y. Panicker, K. Viswanathan, M. Dolezal, C. Van Alsenoy, Arabian J. Chem. (2013) doiorg/101016/jarabjc201308004.
26. J. Lukose, C. Y. Panicker, P. S. Nayak, B. Narayana, B. K. Sarojini, C. Van Alsenoy, A. A. Al-Saadi, Spectrochim. Acta 135 (2015) 608–616.
27. J. B. Bhagyasree, H. T. Varghese, C. Y. Panicker, C. Van Alsenoy, A. A. Al-Saadi, M. Dolezal, J. Samuel, Spectrochim. Acta A 137 (2015) 193–206.
28. B. Servusova, D. Eibinova, M. Dolezal, V. Kubicek, P. Paterova, M. Pesko, K. Kralova, Molecules 17 (2012) 13183.
29. M. A. Matulenko, C. H. Lee, M. Jiang, R. R. Frey, M. D. Cowart, E. K. Bayburt, S. DiDomenico, Bioorg. Med. Chem. 13 (2005) 3705.
30. M. J. Frisch, G. W. Trucks, H. B. Schlegel, G. E. Scuseria, M. A. Robb, J. R. Cheeseman, G. Scalmani, V. Barone, B. Mennucci, G. A. Petersson, H. Nakatsuji, M. Caricato, X. Li, H. P. Hratchian, A. F. Izmaylov, J. Bloino, G. Zheng, J. L. Sonnenberg, M. Hada, M. Ehara, K. Toyota, R. Fukuda, J. Hasegawa, M. Ishida, T. Nakajima, Y. Honda, O. Kitao, H. Nakai, T. Vreven, J. A. Montgomery, Jr., J. E. Peralta, F. Ogliaro, M. Bearpark, J. J. Heyd, E. Brothers, K. N. Kudin, V. N. Staroverov, T. Keith, R. Kobayashi, J. Normand, K. Raghavachari, A. Rendell, J. C. Burant, S. S. Iyengar, J. Tomasi, M. Cossi, N. Rega, J. M. Millam, M. Klene, J. E. Knox, J. B. Cross, V. Bakken, C. Adamo, J. Jaramillo, R. Gomperts, R. E. Stratmann, O. Yazyev, A. J. Austin, R. Cammi, C. Pomelli, J. W. Ochterski, R. L. Martin, K. Morokuma, V. G. Zakrzewski, G. A. Voth, P. Salvador, J. J. Dannenberg, S. Dapprich, A. D. Daniels, O. Farkas, J. B. Foresman, J. V. Ortiz, J. Cioslowski, D. J. Fox, Gaussian 09 (Revision B. 01), Gaussian, Inc., Wallingford CT (2010).
31. J. B. Foresman, E. Frisch, Exploring Chemistry with Electronic Structure Methods: A Guide to Using Gaussian, Gaussian Inc., Pittsburg, PA (1996).
32. R. Dennington, T. Keith, J. Millam, GaussView (Version 5), Semichem Inc., Shawnee Mission KS (2009).
33. J. M. L. Martin, C. Van Alsenoy, GAR2PED, A Program to Obtain a Potential Energy Distribution from a Gaussian Archive Record, University of Antwerp, Belgium (2007).
34. M. Arivazhagan, S. Jeyavijayan, Spectrochim. Acta A 79 (2011) 376–383.
35. R. Renjith, Y. S. Mary, C. Y. Panicker, H. T. Varghese, M. Pakosinska-Parys, C. Van Alsenoy, A. A. Al-Saadi, Spectrochim. Acta 129 (2014) 438.
36. N. B. Colthup, L. H. Daly, S. E. Wiberly, Introduction to Infrared and Raman spectroscopy, Academic Press, New York (1990).
37. P. L. Anto, C. Y. Panicker, H. T. Varghese, D. Philip, O. Temiz-Arpaci, B. Tekiner- Gulbas, I. Yildiz, Spectrochim. Acta 67 (2007) 744.
38. Y. S. Mary, H. T. Varghese, C. Y. Panicker, T. Ertan, I. Yildiz, O. Temiz-Arpaci, Spectrochim. Acta 71 (2008) 566.
39. G. Socrates, Infrared characteristic group frequencies, John Wiley, NewYork (1981).
40. T. Joseph, H. T. Varghese, C. Y. Panicker, K. Viswanathan, M. Dolezal, T. K. Manojkumar, C. Van Alsenoy, Spectrochim. Acta 113 (2013) 203–214.
41. A. Spire, M. Berthes, H. Kallouai, G. De Nunzio, Physica D 137 (2000) 392.
42. M. Barthes, G. De Nunzio, G. Ribet, Synth. Met. 76 (1996) 337.
43. R. Saxena, L. D. Kaudpal, G. N. Malkur, J. Polym Sci A 40 (2002) 3959.
44. Y. S. Mary, H. T. Varghese, C. Y. Panicker, M. Dolezal, Spectrochim. Acta 71 (2008) 725–730.
45. N. P. G. Roeges, A Guide to the Complete Interpretation of IR Spectra of Organic Compounds, Wiley, New York (1994).
46. G. Varsanyi, Assignments of Vibrational Spectra of Seven Hundred Benzene Derivatives, Wiley, New York (1974).
47. M. Kaur, Y. S. Mary, C. Y. Panicker, H. T. Varghese, H. S. Yathirajan, K. Byrappa, C. Van Alsenoy, Spectrochim. Acta 120 (2014) 445–455.
48. H. Endredi, F. Billes, S. Holly, J. Mol. Struct. THEOCHEM 633 (2003) 73.
49. S. Breda, I. D. Reva, L. Lapinski, M. J. Nowak, and R. Fausto, J. Mol. Struct. 786 (2006) 193.
50. S. Akyuz, J. Mol. Struct. 651 (2003) 541.
51. A. Pawlukojc, I. Natkaniec, Z. Malarski, J. Leciejewicz, J. Mol. Struct. 516 (2000) 7.
52. T. Joseph, H. T. Varghese, C. Y. Panicker, K. Viswanathan, N. Sundaraganesan, N. Subramanina, M. Dolezal, Global J. Anal Chem 3 (2012) 1–12.
53. W. He, G. Zhon, J. Li, A. Tian, J. Mol. Struct. THEOCHEM 668 (2004) 201.
54. P. Anbarasu, M. Arivazhagan, Indian J. Pure Appl. Phys. 49 (2011) 227.
55. A. Spire, M. Barthes, H. Kallouai, G. De Nunzio, Physica D 137 (2000) 392–396.
56. C. Y. Panicker, H. T. Varghese, T. Thansani, Turk. J. Chem. 33 (633) –.
57. L. Ushakumari, C. Y. Panicker, H. T. Varghese, A. Haseena, V. Vaidyan, N. Sudhakaran, K. Raju, Orient. J. Chem. 24 (2008) 849.
58. N. Choudhary, S. Bee, A. Gupta, P. Tandon, Comput Theor Chem 1016 (2013) 8–21.
59. B. Kosar, C. Albayrak, Spectrochim. Acta 78A (2011) 160–167.
60. N. Sinha, O. Prasad, V. Narayan, S. R. Shukla, Mol. Simul. 37 (2011) 153–163.
61. G. Gece, Corros. Sci. 50 (2008) 2981–2992.
62. R. J. Parr, L. V. Szentpaly, S. Liu, J. Am. Chem. Soc. 121 (1999) 1922–1924.
63. E. Scrocco, J. Tomasi, Adv. Quantum Chem. 103 (1978) 115.
64. F. J. Luque, J. M. Lopez, M. Orozco, Theor. Chem. Acc. 103 (2000) 343.
65. P. Politzer, J. S. Murray, Chapter 13, In: D. L. Beve ridge, R. Lavery (Eds.), Theoretical Biochemistry and Molecular Biophysics, Springer, Berlin (1991).
66. E. Scrocco, J. Tomasi, Top. Curr. Chem. 42 (1973) 95.
67. S. Moro, M. Bacilieri, C. Ferrari, G. Spalluto, Curr Drug Discov. Technol 2 (2005) 13–21.
68. E. D. Glendening, A. E. Reed, J. E. Carpenter, F. Weinhold, NBO (Version 3. 1), Gaussian Inc., Pittsburg, PA.
69. Y. R. Shen, The Principles of Nonlinear Optics, Wiley, New York (1984).
70. P. V. Kolinsky, Opt. Eng. 31 (1992) 1676–1684.
71. D. F. Eaton, Science 25 (1991) 281–287.
72. D. A. Kleinman, Phys. Rev. 126 (1962) 1977–1979.

73. M. Adant, M. Dupuis, J. L. Bredas, Int. J. Quantum Chem. 56 (1995) 497–507.
74. M. V. S. Prasad, N. Udaya Sri, A. Veeraiah, V. Veeraiah, K. Chaitanya, J. At Mol Sci 4 (2013) 1.
75. G. Mahalakshmi, V. Balachandran, Spectrochim. Acta 131 (2014) 587–598.
76. R. S. Mulliken, J. Chem. Phys. 23 (1955) 1833–1840.
77. K. Wolinski, J. F. Hinton, P. Pulay, J. Am. Chem. Soc. 112 (1990) 8251–8260.
78. T. Premkumar, S. Govindarajan, World J. Microbiol. Biotechnol. 21 (2005) 479.
79. C. G. Bonde, N. J. Gaikwad, Bioorg. Med. Chem. 12 (2004) 2151.
80. R. J. Heath, Y. T. Yu, M. A. Shapiro, E. Olson, C. O. Rock, J. Biol. Chem. 273 (1998) 30316.
81. J. C. Sacchettini, E. J. Rubin, J. S. Freundlich, Nat. Rev. Microbiol. 6 (2008) 41.
82. W. H. J. Ward, G. A. Holdgate, S. Rowsell, E. G. McLean, R. A. Pauptit, E. Clayton, W. W. Nichols, J. G. Colls, C. A. Minshull, D. A. Jude, A. Mistry, D. Timms, R. Camble, N. J. Hales, C. J. Britton, I. W. F. Taylor, Biochemistry-us 38 (199) 12514.
83. Trott, A. J. Olson, J. Comput. Chem. 31 (2010) 455.

Cite this article as:

K. S. Resmi *et al.*: **FT-IR, FT-Raman, NBO, HOMO-LUMO analysis and molecular docking study of 5-chloro-*N*-(2-fluorophenyl)pyrazine-2-carboxamide.** Sci. Lett. 2015, **4**: 216

Appendix

Table 1. Optimized geometrical parameters (B3LYP/6-31++G (6D, 7F)) of 5-chloro-N-(3-chlorophenyl)pyrazine-2-carboxamide, atom labelling according Fig. 3.

Bond Length (Å)					
C1-C2	1.4004	C1-N6	1.3557	C1-H7	1.0832
C2-N3	1.3572	C2-C10	1.5004	N3-C4	1.3431
C4-C5	1.4032	C4-H8	1.0820	C5-N6	1.3245
C5-Cl9	1.8106	C10-O11	1.2423	C10-N12	1.3827
N12-C13	1.4260	N12-H23	1.0117	C13-C14	1.3988
C13-C15	1.4029	C14-C16	1.3884	C14-F24	1.4002
C15-C17	1.4000	C15-H18	1.0854	C16-C19	1.4010
C16-H20	1.0834	C17-C19	1.4018	C17-H21	1.0847
C19-H22	1.0847				
Bond Angle (°)					
C2-C1-N6	121.0	C2-C1-H7	122.5	N6-C1-H7	116.5
C1-C2-N3	120.8	C1-C2-C10	121.9	N3-C2-C10	117.1
C2-N3-C4	118.0	N3-C4-C5	120.1	N3-C4-H8	117.9
C5-C4-H8	122.0	C4-C5-N6	122.9	C4-C5-Cl9	119.3
N6-C5-Cl9	117.8	C1-N6-C5	117.2	C2-C10-O11	122.2
C2-C10-N12	114.5	O11-C10-N12	123.3	C10-N12-C13	123.2
C10-N12-H23	118.9	C13-N12-H23	117.7	N12-C13-C14	120.8
N12-C13-C15	121.3	C14-C13-C15	117.8	C13-C14-C16	122.8
C13-C14-F24	118.6	C16-C14-F24	118.6	C13-C15-C17	120.5
C13-C15-H18	118.8	C17-C15-H18	120.6	C14-C16-C19	118.5
C14-C16-H20	119.5	C19-C16-H20	121.9	C15-C17-C19	120.1
C15-C17-H2	1119.7	C19-C17-H21	120.1	C16-C19-C17	120.1
C16-C19-H22	119.6	C17-C19-H22	120.3		

Table 2. Calculated (scaled) wavenumbers, IR, Raman bands and assignments of 5-chloro-N-(2-fluorophenyl)pyrazine-2-carboxamide.

B3LYP/6-31G(6D, 7F)			B3LYP/6-31++G (6D, 7F)			IR	Raman	Assignments[a]
$\upsilon(cm^{-1})$	IR_I	R_A	$\upsilon(cm^{-1})$	IR_I	R_A	$\upsilon(cm^{-1})$	$\upsilon(cm^{-1})$	-
3479	20.84	97.58	3398	85.63	190.22	3352,3423	3390	υNH(99)
3125	2.86	148.08	3149	5.79	45.62	-	-	υCHPh(98)

3122	4.26	203.92	3143	1.49	72.98	-	-	υCHPz(99)
3110	11.96	67.50	3126	3.07	95.80	-	3130	υCHPz(99)
3107	16.74	144.09	3117	4.73	215.56	-	3113	υCHPh(97)
3093	9.56	88.43	3101	16.13	152.34	-	-	υCHPh(99)
3081	3.28	46.18	3085	3.69	72.92	3085	3076	υCHPh(95)
1653	132.67	159.83	1610	65.19	910.84	1620	1603	υPh(50), υC=O(12)
1606	2.22	104.15	1596	159.92	18.83	1593	1585	υC=O(47), υPh(20)
1587	7.99	8.63	1576	123.46	8.70	1571	1575	υPh(49), δNH(16)
1505	17.24	201.97	1526	421.09	1080.32	-	1530	δNH(42), υCN(42)
1502	36.14	35.83	1514	26.39	277.64	1515	1509	υPz(45), δCHPz(18)
1495	46.29	20.72	1491	49.72	123.74	1483	-	υPz(77)
1482	289.09	156.29	1468	42.80	49.79	-	1474	δCHPh(19), υPh(48)
1444	68.01	48.60	1444	98.95	103.81	1454	1447	υPh(45), δCHPh(25)
1425	161.74	1.24	1417	123.80	71.63	1422	1405	δCHPz(56), υPz(21)
1320	40.99	39.87	1333	82.11	642.78	1320	1346	υPh(63), υCN(14)
1287	5.59	2.32	1297	11.20	259.22	-	1301	δCHPz(39), δCHPh(14)
1276	77.19	46.70	1291	20.67	132.98	1288	-	υPz(45), υCC(12)
1267	33.47	1.45	1271	1.06	5.41	-	1270	δCHPh(56), υPz(13)
1262	49.97	169.47	1245	42.79	299.07	1250	-	δNH(40), υCN(39)
1250	2.28	26.11	1240	49.55	53.41	-	1238	υPz(42), δCHPz(17)
1204	23.50	3.03	1195	0.62	19.17	1187	1191	υPz(91)

1198	0.51	3.40	1170	1.05	31.17		-	1167	δCHPh(82)
1172	0.79	5.69	1153	17.58	10.76		1140	1148	δCHPh(37), υCF(20)
1119	253.49	9.26	1126	105.87	4.74		1114	1126	υCN(22), δPz(15)
1105	46.82	9.02	1089	141.67	31.12	1090	1082		υPz(27), υCCl(12)
1082	28.25	5.89	1074	13.47	7.42		1066	-	δCHPh(39)
1028	1.99	24.46	1023	14.21	53.36		1021	1019	υPh(70), δCHPh(21)
981	36.10	2.17	994	2.10	0.57		993	-	γCHPh(81), δPh(36)
977	0.00	0.44	983	38.63	8.36		978	-	δPz(49), υPz(32)
946	1.99	3.60	954	6.46	1.00		-	957	γCHPz(74)
940	4.72	3.12	953	5.15	0.11		945	-	γCHPh(79)
918	9.43	1.33	915	6.00	0.58		926	914	γCHPz(84)
893	10.57	6.69	875	36.59	19.48		-	892	υCN(19), δC=O(19)
855	6.04	5.21	872	2.70	0.19		-	857	γCHPh(78)
849	25.97	6.23	836	7.14	2.08		843	-	δPh(37), υCN(17)
797	3.66	8.71	832	113.29	1.53		823	-	γNH(53), τC=O(15)
779	16.45	3.67	785	4.18	2.49		-	797	τPz(55), γCC(20)
754	73.53	3.22	782	7.45	0.76		-	779	δPz(29), υCF(15)
746	12.68	32.24	760	82.53	0.48		754	764	γCHPh(94)
713	9.24	5.23	733	14.49	56.81		-	-	δPh(20), δPz(19)
693	1.67	0.13	722	1.83	1.15		715	713	τPh(59), δPh(16)
615	1.41	7.78	696	0.13	1.05		-	692	υCCl(52),

								τPz(17)
605	2.20	5.47	623	1.96	10.82	-	614	δPz(82)
561	34.23	9.29	592	4.87	10.89	591	598	δPh(69)
538	9.49	2.97	556	0.86	0.25	548	550	τPh(59), γCN(15)
534	1.75	5.02	531	19.01	3.40	-	528	δPh(26), δCN(28)
517	57.06	35.07	501	3.34	0.05	518	521	τPz(37), γCCl(29), γCC(18)
468	11.28	6.97	498	4.78	0.98	490	492	δPh(24), υCCl(19), δCC(14)
454	27.14	0.93	453	7.40	0.09	453	453	τPh(53), γCF(27)
443	2.15	0.62	444	4.58	1.11	-	437	δCF(49), δC=O(11)
414	15.62	0.55	418	17.24	0.17	414	417	τPz(79)
375	9.80	3.96	405	35.85	11.59	-	380	γCCl(30), δC=O(12)
336	4.19	2.42	327	0.10	0.08	-	334	τPh(31), γCF(14)
300	7.17	3.61	305	2.77	4.39	-	317	δCCl(26), δPz(22)
292	0.73	2.36	271	0.07	2.96	-	286	δCN(35), δCCl (31)
255	1.44	2.68	267	0.89	2.64	-	265	γCC(22), γCF(19)
216	1.83	2.05	206	0.68	1.28	-	201	δCN(16), δCC(13)
188	1.36	4.62	199	1.89	1.89	-	183	τPh(64)
133	4.42	3.84	172	11.55	0.41	-	-	δCN(46), δCC(19)
100	0.89	1.74	102	1.63	1.61	-	127	τCC(42), τCN(23)

77	4.66	3.69	88	4.93	2.04	-	95	τPz(47), τC=O(17)
47	0.11	2.48	61	0.20	0.67	-	60	δCC(25), δCN(59)
37	0.26	11.57	45	1.03	0.62	-	-	τCN(44), τCC(40)
29	0.34	3.07	33	0.61	0.36	-	-	τC=O(38), τPz(12)

[a] PED (%) is given in the brackets in the assignment column;υ-stretching; δ-in-plane deformation; γ-out-of-plane deformation; τ-twisting; Ph-phenyl ring; Pz-pyrazine ring; IR_I – IR intensity; R_A – Raman activity.

Table 3. Second-order perturbation theory analysis of Fock matrix in NBO basis corresponding to the intramolecular bonds of the title compound.

Donor(i)	Type	ED/e	Acceptor(j)	Type	ED/e	E(2)[a]	E(j)-E(i)[b]	F(i,j)[c]
C1-C2	σ	1.987	C2-N3	σ*	0.021	1.30	1.23	0.036
			C2-C10	σ*	0.077	1.64	1.15	0.039
			C10-O11	σ*	0.027	1.56	1.28	0.040
C2-C10	σ	1.975	C1-C2	σ*	0.040	1.56	1.20	0.039
			C1-N6	σ*	0.016	2.54	1.16	0.049
			N3-C4	σ*	0.014	3.10	1.18	0.054
			N12-C13	σ*	0.028	3.70	1.08	0.056
C4-C5	σ	1.992	C5-N6	σ*	0.028	1.57	1.27	0.040
C5-Cl9	σ	1.987	C1-N6	σ*	0.016	3.28	1.16	0.055
			N3-C4	σ*	0.014	2.75	1.19	0.051
C5-N6	π	1.729	C1-C2	π*	0.298	20.36	0.34	0.075
			N3-C4	π*	0.306	16.57	0.32	0.066
C10-N12	σ	1.987	C2-N3	σ*	0.021	1.27	1.30	0.036
			N12-C13	σ*	0.028	1.61	1.22	0.040
			C13-C15	σ*	0.023	1.38	1.38	0.039
C10-O11	σ	1.995	C1-C2	σ*	0.039	1.21	1.51	0.038
			C2-C10	σ*	0.078	1.16	1.40	0.037
C13-C14	σ	1.977	N12-C13	σ*	0.028	1.24	1.13	0.033

			C13-C15	σ*	0.023	3.15	1.28	0.057
			C14-C16	σ*	0.023	3.03	1.29	0.056
C13-C15	σ	1.972	C10-N12	σ*	0.083	1.69	1.14	0.040
			N12-C13	σ*	0.028	1.21	1.11	0.033
			C13-C14	σ*	0.039	3.40	1.25	0.058
			C14-F24	σ*	0.030	3.84	0.94	0.054
			C15-C17	σ*	0.014	2.42	1.28	0.050
C13-C15	π	1.681	C10-N12	σ*	0.083	2.07	0.70	0.036
			C14-C16	π*	0.362	21.02	0.29	0.070
			C17-C19	π*	0.339	18.26	0.29	0.065
C14-C16	σ	1.981	N12-C13	σ*	0.028	3.55	1.12	0.057
			C13-C14	σ*	0.039	3.50	1.26	0.060
			C16-C19	σ*	0.015	2.21	1.29	0.048
C14-C16	π	1.663	C13-C15	π*	0.389	19.47	0.29	0.067
			C17-C19	π*	0.339	20.09	0.29	0.069
LP N3	σ	1.917	C1-C2	σ*	0.040	9.30	0.89	0.082
			C2-C10	σ*	0.077	2.18	0.77	0.037
			C4-C5	σ*	0.046	9.72	0.87	0.083
LPN6	σ	1.995	C1-C2	σ*	0.040	8.94	0.90	0.081
			C4-C5	σ*	0.046	9.78	0.88	0.084
			C5-Cl9	σ*	0.075	5.04	0.46	0.043
LPCl9	σ	1.995	C4-C5	σ*	0.046	1.12	1.43	0.036
LPCl9	π	1.971	C4-C5	σ*	0.046	3.02	0.83	0.045
			C5-N6	σ*	0.028	5.06	0.83	0.058
LPCl9	n	1.924	C5-N6	π*	0.392	13.23	0.29	0.06
LPO11	σ	1.978	C2-C10	σ*	0.077	2.40	1.09	0.046
			C10-N12	σ*	0.083	2.09	1.12	0.044
LPO11	π	1.857	C2-C10	σ*	0.077	20.35	0.64	0.104
			C10-N12	σ*	0.083	25.83	0.67	0.120
LPN12	σ	1.708	C10-O11	σ*	0.027	2.56	0.81	0.044
			C10-O11	π*	0.259	44.07	0.31	0.105
			C13-C14	σ*	0.039	4.07	0.81	0.055
			C13-C15	σ*	0.023	3.75	0.83	0.053
			C13-C15	π*	0.389	13.30	0.29	0.057
LPF24	σ	1.990	C13-C14	σ*	0.039	1.17	1.58	0.039

			C14-C16	σ*	0.023	1.36	1.60	0.042
LPF24	π	1.968	C13-C14	σ*	0.039	6.45	0.93	0.069
			C14-C16	σ*	0.023	5.35	0.96	0.064
LPF24	n	1.922	C14-C16	π*	0.362	17.62	0.41	0.082

[a]E(2) means energy of hyper-conjugative interactions (stabilization energy in kJ/mol)

[b]Energy difference (a.u) between donor and acceptor i and j NBO orbitals

[c]F(i,j) is the Fock matrix elements (a.u) between i and j NBO orbitals

Table 4. NBO results showing the formation of Lewis and non-Lewis orbitals.

Bond(A-B)	ED/e[a]	EDA%	EDB%	NBO	s%	p%	
σC1-C2	1.98732	49.18	50.82	0.7013($sp^{1.68}$)C+	37.24	62.76	
	-0.75554	-	-	0.7129($sp^{1.70}$)C	37.09	62.91	
σC2-C10	1.97468	52.36	47.64	0.7236($sp^{2.06}$)C+	32.65	67.15	
	-0.68366	-	-	0.6902($sp^{1.83}$)C	35.32	64.68	
σC4-C5	1.99227	49.06	50.94	0.7004($sp^{1.78}$)C+	35.94	64.06	
	-0.77251	-	-	0.7137($sp^{1.37}$)C	42.14	57.86	
σC5-Cl9	1.98698	45.46	54.54	0.6742($sp^{3.28}$)C+	23.33	76.67	
	-0.68814	-	-	0.7385($sp^{5.57}$)Cl	15.15	84.85	
πC5-N6	1.72864	44.74	55.26	0.6689($sp^{1.00}$)C	0.00	100.0	
	-0.34978	-	-	0.7433($sp^{1.00}$)N	0.00	100.0	
σC10-N12	1.98715	36.87	63.13	0.6072($sp^{2.19}$)C+	31.35	68.65	
	-0.82794	-	-	0.7946($sp^{1.77}$)N	36.14	63.86	
σC10-O11	1.99455	35.28	64.72	0.5939($sp^{2.17}$)C	31.53	68.47	
	-0.99733	-	-	0.8045($sp^{1.68}$)O	37.13	62.87	
σC13-C14	1.97651	51.39	48.61	0.7169($sp^{1.85}$)C+	35.11	64.89	
	-0.73011			0.6972($sp^{1.61}$)C	38.25	61.75	
σC13-C15	1.97180	51.22	48.78	0.7156($sp^{1.70}$)C+	37.04	62.96	
	-0.71427	-	-	0.6985($sp^{1.91}$)C	34.32	65.68	
πC13-C15	1.68125	52.00	48.00	0.7211($sp^{99.99}$)C+	0.02	99.98	
	-0.26993	-	-	0.6928($sp^{1.00}$)C	0.00	100	
σC14-C16	1.98099	49.86	50.14	0.7061($sp^{1.51}$)C+	39.77	60.23	
	-0.72675	-	-	0.7081($sp^{1.96}$)C	33.77	66.23	
πC14-C16	1.66288	49.05	50.95	0.7003($sp^{1.00}$)C+	0.01	99.99	-0.272
				0.7138($sp^{1.00}$)C	0.00	100	

n1 N3	1.91734	-	-	$sp^{2.32}$	30.08	69.92
	-0.37527					
n1 N6	1.90063	-	-	$sp^{2.50}$	28.53	71.47
	-0.37965					
n1 Cl9	1.99480	-	-	$sp^{0.18}$	84.96	15.04
	-0.92782					
n2 Cl9	1.97079	-	-	$sp^{99.99}$	0.11	99.89
	-0.32964					
n3 Cl9	1.92371	-	-	$sp^{1.00}$	0.00	100
	-0.32940					
n1 O11	1.97848	-	-	$sp^{0.64}$	61.03	38.98
	-0.68834					
n2 O11	1.85716	-	-	$sp^{1.00}$	0.01	99.99
	-0.24503					
n1 N12	1.70790	-	-	$sp^{99.99}$	0.44	99.56
	-0.27690					
n1 F24	1.98953	-	-	$sp^{0.38}$	72.51	27.49
	-1.04259					
n2 F24	1.96822	-	-	$sp^{99.99}$	0.04	99.96
	-0.39775					
n3 F24	1.92224	-	-	$sp^{1.00}$	0.01	99.99
	-0.39494	-	-	-	-	-

[a] ED/e is expressed in a.u.

Table 5. The charge distribution calculated by the Mulliken and natural bond orbital (NBO)methods.

Atom	Mulliken charge	Natural charge
1C	0.014982	0.00449
2C	0.188916	0.07346
3N	-0.399910	-0.36540
4C	0.060994	-0.00834
5C	0.115066	0.17855
6N	-0.378441	-0.41662
7H	0.176642	0.24235
8H	0.186460	0.25014
9Cl	0.003799	-0.01128

10C	0.580560	0.66177
11O	-0.472311	-0.55956
12N	-0.714232	-0.65108
13C	0.260962	0.07981
14C	0.377411	0.42339
15C	-0.164714	-0.23223
16C	-0.196538	-0.28980
17C	-0.138398	-0.24125
18H	0.141947	0.24297
19C	-0.123845	-0.22230
20H	0.158621	0.25761
21H	0.141564	0.24398
22H	0.145180	0.24475
23H	0.336503	0.42450
24F	-0.301218	-0.32991

Table 6. Calculated Mulliken charges of 5-chloro-N-(2-fluorophenyl) pyrazine-2-carboxamide

Atom	B3LYP/6-31G (6D, 7F)	B3LYP/6-31++G(6D,7F)
1C	0.027054	-0.133456
2C	0.101425	-0.191372
3N	-0.327057	-0.126246
4C	0.074678	0.280180
5C	-0.090266	-0.407952
6N	-0.318771	-0.101427
7H	0.176417	0.338484
8H	0.198963	0.291115
9Cl	0.123746	0.331561
10C	0.515772	0.231184
11O	-0.389174	-0.537162
12N	-0.742937	-0.516831
13C	0.253605	0.662534
14C	0.317803	-1.088415
15C	-0.116906	0.226787
16C	-0.149597	-0.016771
17C	-0.136188	-0.079519
18H	0.143680	0.270507
19C	-0.110888	-0.333346

20H	0.155867	0.245219
21H	0.141997	0.213496
22H	0.141946	0.191750
23H	0.326723	0.530131
24F	-0.317892	-0.280453

Table 7. Experimental and calculated ^{1}H NMR parameters (with respect to TMS).

Protons	σ_{TMS}	B3LYP/6-31G	$\delta_{calc} = \sigma_{TMS}-\sigma_{calc}$	Exp. δ_{ppm}
7 H	32.7711	22.7130	9.1614	9.26
8 H		23.8299	8.9411	8.60
18 H		23.3984	9.3726	8.51
20 H		25.4877	7.2833	7.09
21 H		25.3130	7.4580	7.24
22 H		25.4883	7.2827	7.09
23 H		22.4336	10.3374	9.79

Table 8. The binding affinity values of different poses of the 5-chloro-N-(2-fluorophenyl)pyrazine-2-carboxamide predicted by Autodock Vina.

Mode	Affinity (kcal/mol)	Distance from best mode (Å)	
-	-	RMSD l.b.	RMSD u.b.
1	7.4	0.000	0.000
2	7.2	1.266	1.288
3	7.2	1.0125	1.620
4	7.0	1.519	1.681
5	7.0	1.465	1.538
6	6.8	1.872	2.258
7	6.8	4.457	5.197
8	6.7	4.434	5.088
9	6.7	8.148	11.195